AFRL-PR-WP-TP-2006-202

DEPOSITION OF ($Y_2BaCuO_5/YBa_2Cu_3O_{7-x}$) X N MULTILAYER FILMS ON Ni-BASED TEXTURED SUBSTRATES

T.J. Haugan, P.N. Barnes, T.A. Campbell, A. Goyal, A. Gapud, L. Heatherly, and S. Kang

JANUARY 2005

PROPULSION DIRECTORATE
AIR FORCE MATERIEL COMMAND
AIR FORCE RESEARCH LABORATORY
WRIGHT-PATTERSON AIR FORCE BASE, OH 45433-7251

REPORT DOCUMENTATION PAGE

Form Approved OMB No. 0704-0188

1. REPORT DATE ***(DD-MM-YY)***
January 2005

2. REPORT TYPE
Journal Article Postprint

3. DATES COVERED ***(From - To)***
01/10/2004 – 01/10/2005

4. TITLE AND SUBTITLE
DEPOSITION OF ($Y_2BaCuO_5/YBa_2Cu_3O_{7-X}$) X *N* MULTILAYER FILMS ON Ni-BASED TEXTURED SUBSTRATES

5a. CONTRACT NUMBER
In-house

5b. GRANT NUMBER

5c. PROGRAM ELEMENT NUMBER
61102F/62203F

5d. PROJECT NUMBER
3145

5e. TASK NUMBER
32

5f. WORK UNIT NUMBER
ZE

6. AUTHOR(S)
T.J. Haugan, P.N. Barnes, and T.A. Campbell (AFRL/PRPG)
A. Goyal, A. Gapud, L. Heatherly, and S. Kang (Oak Ridge National Laboratory)

7. PERFORMING ORGANIZATION NAME(S) AND ADDRESS(ES)
Power Generation Branch (AFRL/PRPG)
Power Division
Propulsion Directorate
Air Force Research Laboratory, Air Force Materiel Command
Wright-Patterson Air Force Base, OH 45433-7251

Oak Ridge National Laboratory
1 Bethel Valley Road
Building 4500S, Room No. S-250
Oak Ridge, TN 37831-6116

8. PERFORMING ORGANIZATION REPORT NUMBER
AFRL-PR-WP-TP-2006-202

9. SPONSORING/MONITORING AGENCY NAME(S) AND ADDRESS(ES)
Propulsion Directorate
Air Force Research Laboratory
Air Force Materiel Command
Wright-Patterson AFB, OH 45433-7251

10. SPONSORING/MONITORING AGENCY ACRONYM(S)
AFRL-PR-WP

11. SPONSORING/MONITORING AGENCY REPORT NUMBER(S)
AFRL-PR-WP-TP-2006-202

12. DISTRIBUTION/AVAILABILITY STATEMENT
Approved for public release; distribution is unlimited.

13. SUPPLEMENTARY NOTES

PAO case number: ASC 03-1851; Date cleared: 14 Nov 2003. Paper contains color.

Journal article postprint published in Physica C, Vol. 425 (2005).

14. ABSTRACT
Deposition of ($Y_2BaCuO_{5-0.5\,nm}/YBa_2Cu_3O_{7-x\sim 15\,nm}$) X *N* multilayer films on rolling-assisted biaxially textured Nialloy (RABiTS^{TM}) substrates was investigated, as a new candidate coated conductor architecture for improved flux pinning. Significant enhancements of critical current density (J_c) > 6-fold were measured for applied magnetic fields up to 7 T at 77 K, for multilayer films compared to $YBa_2Cu_3O_{7-x}$—only films. By comparing $J_c(H)/J_c(0\ T)$ plots of films deposited on RABiTS and single-crystal substrates, the relative increase of $J_c(H)$ from pinning was the same as measured on both substrates. This indicates the varying microstructural properties of the RABiTS templates were, on average, not adversely affecting the pinning enhancements.

15. SUBJECT TERMS
flux pinning, nanoparticle, YBCO, coated conductor

16. SECURITY CLASSIFICATION OF: a. REPORT	b. ABSTRACT	c. THIS PAGE	17. LIMITATION OF ABSTRACT:	18. NUMBER OF PAGES	19a. NAME OF RESPONSIBLE PERSON (Monitor)
Unclassified	Unclassified	Unclassified	SAR	12	Paul N. Barnes
					19b. TELEPHONE NUMBER *(Include Area Code)* N/A

Standard Form 298 (Rev. 8-98)
Prescribed by ANSI Std. Z39-18

Available online at www.sciencedirect.com
SCIENCE DIRECT®
ELSEVIER
Physica C 425 (2005) 21–26
PHYSICA C
www.elsevier.com/locate/physc

Deposition of $(Y_2BaCuO_5/YBa_2Cu_3O_{7-x}) \times N$ multilayer films on Ni-based textured substrates

T.J. Haugan [a,*], P.N. Barnes [a], T.A. Campbell [a], A. Goyal [b], A. Gapud [b], L. Heatherly [b], S. Kang [b]

[a] *Air Force Research Laboratory, Propulsion Directorate, 1950 Fifth Street Building 450, Wright-Patterson AFB, OH 45433-7251, United States*
[b] *Oak Ridge National Laboratory, 1 Bethel Valley Road, Building 4500S, Room No. S-250, Oak Ridge, TN 37831-6116, United States*

Received 10 January 2005
Available online 1 July 2005

Abstract

Deposition of $(Y_2BaCuO_{5\text{–}0.5\ \mathrm{nm}}/YBa_2Cu_3O_{7-x\sim15\ \mathrm{nm}}) \times N$ multilayer films on rolling-assisted biaxially textured Ni-alloy (RABiTS[TM]) substrates was investigated, as a new candidate coated conductor architecture for improved flux pinning. Significant enhancements of critical current density (J_c) > 6-fold were measured for applied magnetic fields up to 7 T at 77 K, for multilayer films compared to $YBa_2Cu_3O_{7-x}$—only films. By comparing $J_c(H)/J_c(0\ \mathrm{T})$ plots of films deposited on RABiTS and single-crystal substrates, the relative increase of $J_c(H)$ from pinning was the same as measured on both substrates. This indicates the varying microstructural properties of the RABiTS templates were, on average, not adversely affecting the pinning enhancements.

PACS: 74.60.−w; 74.60.Ge; 74.60.Jg; 74.62.−c; 74.80.Fp

Keywords: Flux pinning; Nanoparticle; YBCO; Coated conductor

1. Introduction

The development of $YBa_2Cu_3O_{7-x}$ (YBCO or 123) thick films on buffer-coated Ni-alloy substrates (coated conductors) with $J_c > 1\ \mathrm{MA/cm^2}$ offers great promise for incorporation into power applications such as generators or motors, operating at 77 K [1–13]. The RABiTS process is used to introduce a high degree of grain alignment in the Ni-alloys, that is epitaxially transferred into the buffer and 123 film layers [7–10]. Efforts to improve the J_c of coated conductors by increasing

* Corresponding author. Tel.: +1937 255 7163; fax: +1937 656 4095.
E-mail address: timothy.haugan@wpafb.af.mil (T.J. Haugan).

0921-4534/$ - see front matter
doi:10.1016/j.physc.2005.05.013

flux pinning have only recently been initiated [2,3]. This paper presents new improvements of flux pinning of coated conductors, by applying a recently developed method to incorporate dispersions of Y_2BaCuO_5 (211) nanoparticles into YBCO by multilayer deposition [14,15].

Growth of $(211/123) \times N$ multilayer films was shown to increase J_c (77 K,∼1–2 T) of YBCO by a factor of 2–3, when deposited on single crystal substrates [14,15]. The $(211/123) \times N$ films are a superlattice-type structure of alternating layers of 123 and 211 'pseudo-layers' containing discontinuous 211 nanoparticles that deposit by the island growth method. The 211 nanoparticle size is as small as ∼8 nm with areic number density estimated as $>4 \times 10^{11}$ particles/cm^2 [15]. The resulting composite structure is essentially a layered dispersion of non-superconducting 211 nanoparticles inside a 123 matrix.

The issues of how $(211/123) \times N$ films will deposit onto RABiTS substrates have not been addressed thus far. RABiTS substrates have unique features compared to single crystal substrates which affect the growth and properties of films deposited on them: Ni grains that are not completely *c*-axis oriented but tilted out-of-the-plane typically ±0–8°, and higher angle grain boundaries (GBs) typically with total misorientations of 0–7°. Grain boundaries with in-plane misorientations greater than 5° are expected to result in reduced critical currents, whereas lower-angle GB's may in-fact act as flux-pinning sites. The GB's are multifaceted structures at the intersection of irregular-shaped grains that are misaligned both in-the-plane and tilted out-of-the-plane. How these Ni-alloy template structures affect the $(211/123) \times N$ composite film coatings will be presented in this paper.

2. Experimental

Buffered $Ni_{0.97}W_{0.03}$ (Ni–W) substrates were prepared at Oak Ridge National Laboratory (ORNL) and American Superconductor Corporation (AMSC) using similar procedures [11], and buffered Ni substrates were prepared at Air Force Research Laboratory (AFRL) [16]. The buffer layer architecture on Ni–W was a cap layer of CeO_2 25 nm thick, an intermediate layer of YSZ 200 nm thick, and a seed layer of Y_2O_3 30 nm thick. Y_2O_3 layers were deposited by reactive electron beam evaporation, and YSZ and CeO_2 layers were deposited by an RF magnetron sputtering process [11,16]. Buffered Ni substrates were prepared with a cap layer of CeO_2 ∼70 nm thick, an intermediate layer of YSZ ∼500 nm thick, and a seed layer of CeO_2 ∼70 nm, using pulsed laser deposition (PLD) for all buffer layers [16].

Multilayer $(211/123) \times N$ and 123 films were deposited onto buffer-coated RABiTS substrates by PLD, using conditions described in detail previously [14–17]. Deposition parameters were 248 nm laser wavelength, ∼3.2 J/cm^2 laser fluence, 4 Hz laser repetition rate, 6 cm target-to-substrate distance, 780 °C heater block temperature, 88–90% dense 123-only and 211-only targets, 300 m Torr oxygen partial-pressure, and a post-deposition anneal at 500 °C and 1 atmosphere of oxygen [17]. An automated target rotation and pulse-triggering system was used to control the deposition sequences, with a period of about 13 s during which the deposition was stopped and different targets were rotated into position. The film thickness for every deposition was measured on reference films deposited onto single crystal substrates. The 211 'pseudo-layer' thickness was calculated assuming a smooth continuous layer, although the thin 211 layer consists of discontinuous and discrete nanoparticles. Unless noted otherwise the film thickness was kept in the range 280–350 nm. A 123 reference film was deposited at ORNL with slightly different PLD conditions: 790 °C substrate temperature, 120 m Torr O_2 partial pressure, 308 nm laser wavelength, 4 J/cm^2 fluence, 10 Hz repetition rate, and cooling rate 7 °C/min in 580 m Torr O_2 pressure.

Critical transition temperatures (T_c) and transport $J_c(H)$ measurements were made at ORNL and AFRL, with excellent agreement. A 1 μV/cm criterion was used for J_c. Whole width measurements and macrobridges of about 0.1–0.5 cm width were used for J_c measurements. Characterization of microstructures was performed with scanning electron microscopy (SEM, FEI–Sirion).

3. Results and discussion

Microstructural properties of the film surfaces are shown in Figs. 1 and 2, for different SEM magnifications to demonstrate features at varying length scales. Multilayer films had unique microstructural features compared to 123-only films, that are summarized in the following points.

(1) Void formations 0.1–1 μm in size were notably enhanced for multilayer films compared to 123-only films, as shown in Figs. 1 and 2. Voids were observed as dark-or-black colored defects in SEM micrographs. Void areic number densities were higher for multilayer films than YBCO-only films; $\sim 4\times10^{8}$ defects cm^{-2} compared to $\sim 1\times10^{8}$ defects cm^{-2} respectively, as measured on grains with highest density of voids. Formations of voids occurred particularly on grains with high densities of film-ledge formations, as shown in Fig. 2(b) bottom and left grains. About 30–40% of multilayer film grains showed moderate increase of void densities (e.g. Fig. 1(b) high magnification image, lower-left grain), while less than 10% of the grains showed large increases of void defects enough to presumably limit current flow (Fig. 1(b) high magnification image, bottom–middle grain).

(2) Surface particulate defects, which typically are observed in PLD films as $\sim$0.5 μm size white-color defects (Fig. 1(a) bottom, upper right grain), were greatly reduced with multilayer films. However elimination of these defects is not expected to have a great effect on flux pinning, as their areic number density is very low.

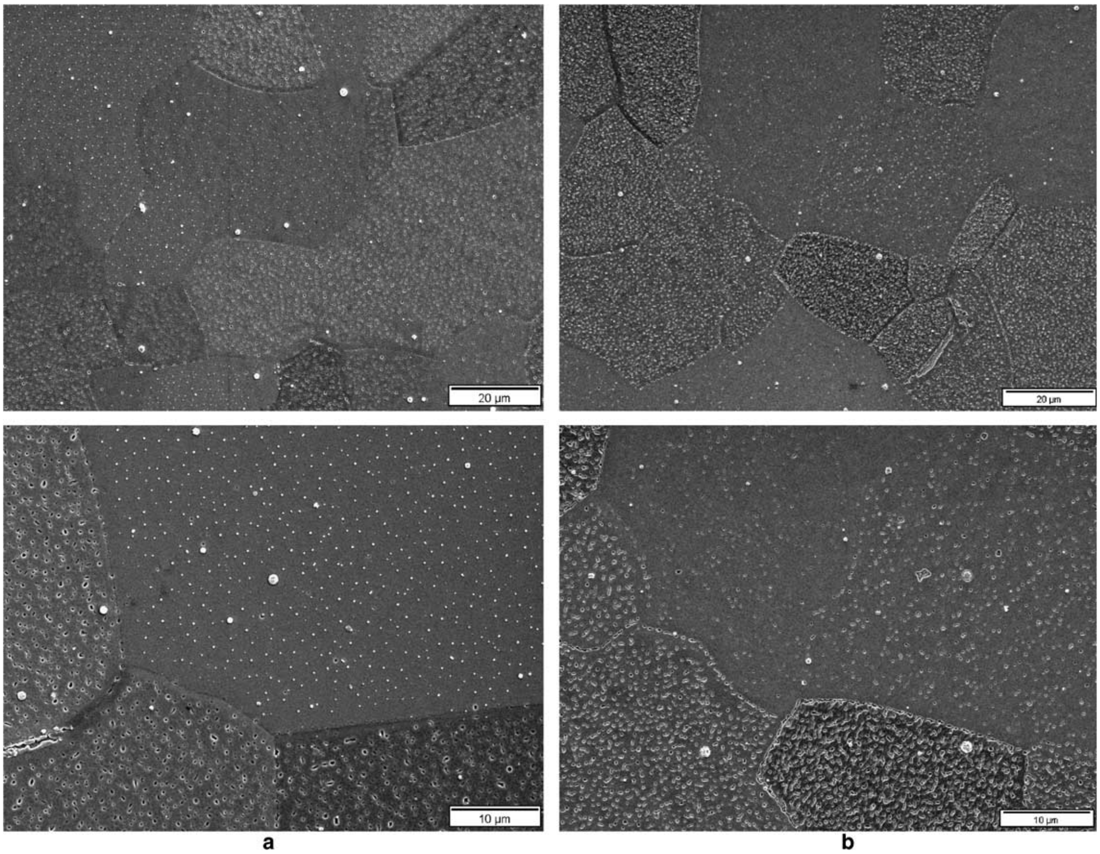

Fig. 1. SEM micrographs of films deposited on ORNL RABiTS substrates: (a) YBCO-only at 1k× (upper) and 2k× (lower) magnifications, and (b) $(211_{\sim 1.0\ nm}/123_{\sim 10.0\ nm})\times 25$ multilayer at similar magnifications.

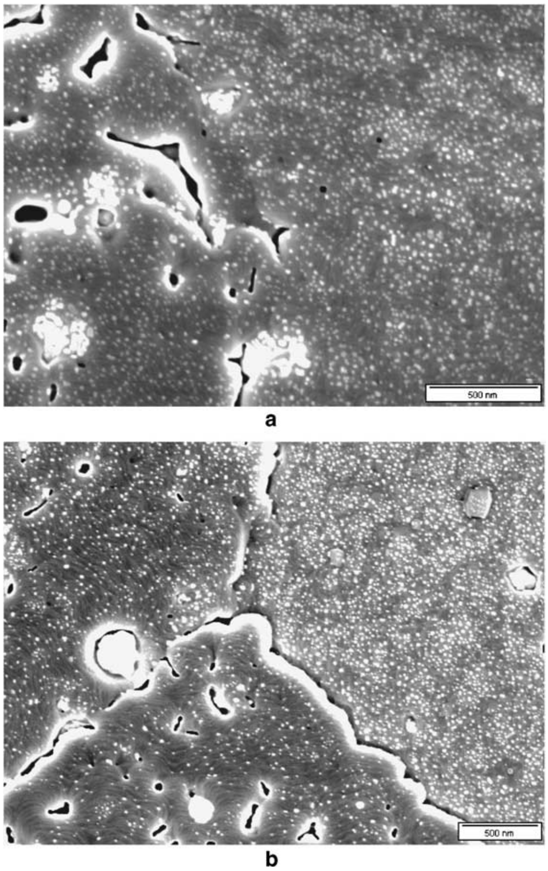

Fig. 2. High magnification SEM micrographs of different grains and grain boundaries of a $(211_{\sim 1.0\ \mathrm{nm}}/123_{\sim 10\ \mathrm{nm}}) \times 26$ film deposited on AMSC RABiTS substrate. Nanoparticles are white-spherical-shaped objects about 10–15 nm in size, and voids are black objects approximately 0.1–1.0 μm in size. Note especially the ∼20–40 nm spaced film-ledge formations in the left-and-bottom grains of (b), and reduced nanoparticle formation and enhanced void formations on those grains. Nanoparticle formation on the right-side grain of (b) is almost exactly similar as on $SrTiO_3$ or $LaAlO_3$ single crystal substrates [15].

(3) Intragrain nanoparticle formations varied noticeably depending on the underlying film and grain structures, as shown in Fig. 2. Nanoparticles were observed as white-color spherical-shaped particles approximately 10–15 nm in diameter with areic number densities $>10^{11}$ particles cm^{-2}, similar as on single crystal substrates [15]. Nanoparticle formations were reduced particularly on grains that exhibited high-densities or close-spacings of film-ledge formations. Film-ledges with close-spacing intervals of about 20–40 nm can be observed by close examination in Fig. 2(b) bottom-and-left grains. The film ledges deposited with such close-spacings presumably indicate the presence of underlying tilted Ni grains. Film ledges are also observed on single crystal substrates, however with much larger spacing of ∼200 nm. The positive or negative effects of depositing multilayer films on tilted substrates are unknown yet, but are being studied in detail [18]. The reason for reduced nanoparticle formations on (tilted) Ni-grains is not precisely known, however could result from non-preferential growth of 211 from relative-tilting of the plume and inclined substrate deposition (ISD) effects [13], or non-preferred growth of 211 at the base of film-ledge sites because of the 2–7% lattice mismatch of 211–123 [15]. The film-ledge bases with 90° step junctions have doubly active 123 film growth surfaces, which may suppress formation of 211 from the vapor phase, whereas the top-edge and top-point-edge of the film-ledge surfaces are energetically attractive sites for 211 coalescence and ripening [15].

(4) Close inspection of grain boundaries (Fig. 2) indicated that nanoparticle formation there was varied, with occasional enhancement at the edges. Some preferential growth at the grain boundaries might be speculated to occur based on the growth processes described above. However only minimal preferential growth was observed, possibly because of the complexity of the grain boundaries.

To summarize the microstructural properties of multilayer films compared to 123-only films, moderate differences were observed on about 30–40% of the grains, and severe differences were noted on <10% of the grains.

Transition temperatures of multilayer $\{(211_{\sim 1.2\ \mathrm{nm}}/123_{\sim 11\ \mathrm{nm}}) \times N,\ N = 20\text{–}25\}$ and 123-only samples were virtually the same ∼89–90 K measured at AFRL by ac susceptibility methods [16] and at ORNL by transport methods. This is slightly different from T_c measurements on single crystals where a small decrease of ∼1–2 K was measured for similar multilayer compared to 123 films [15]. This result suggests the template and/or CeO_2 cap buffer layer is having a noticeable effect on the T_c values.

The effect of multilayer depositions on $J_c(77\ \mathrm{K},H)$ properties are shown in Fig. 3(a). Multilayer films had significantly increased $J_c(H)$ values for $H > 0.3$ T when compared to 123-only films, and the increase was consistently measured for different 211 and 123 thickness parameters.

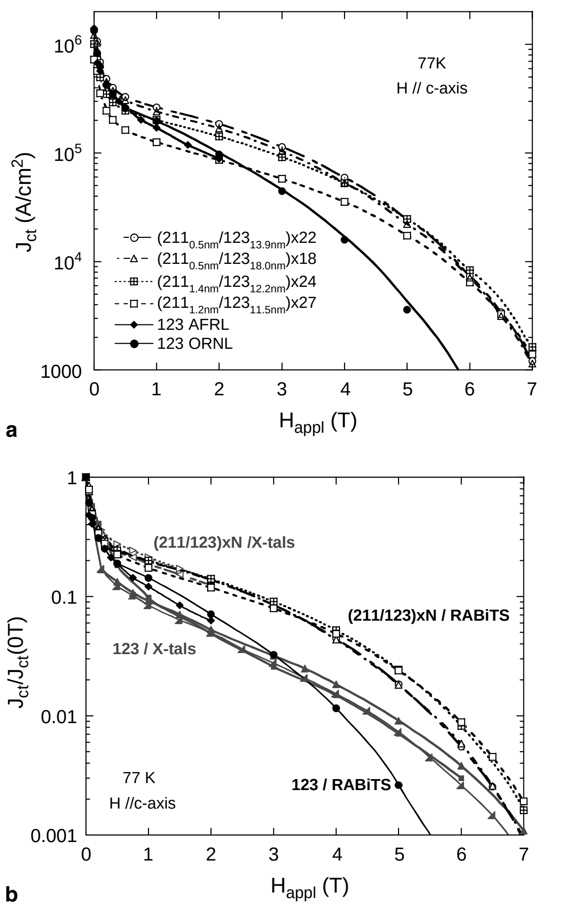

Fig. 3. (a) Transport critical current density (J_{ct}) at 77 K for multilayer films compared to 123 reference films deposited at AFRL and ORNL; all films were deposited on ORNL Ni–W substrates, and (b) normalized J_{ct} measurements for samples from Fig. 3(a) (black) compared to similar samples deposited on single crystal substrates (gray). 123-only films have solid lines and multilayer films are dotted lines: 123 films deposited on $LaAlO_3$ at AFRL (◢, ▲ and processed by the BaF_2 method at ORNL ■ all with $J_c(0\ \mathrm{T})$ from 4 MA/cm^2 to 5 MA/cm^2 [15], and $(211_{0.6\ \mathrm{nm}}/123_{11.7\ \mathrm{nm}}) \times 21$ on $LaAlO_3$ (ω,ϖ) with $J_c(0\ \mathrm{T})$ from 4 MA/cm^2 to 4.5 MA/cm^2 [15]. One film with the lowest J_c (□) was noticeably bent, which could have lowered $J_c(H)$ for all H values. J_c was calculated using the entire film thickness.

The increase of $J_c(H)$ was 2-fold at 2 T, and greater than 6-fold at fields of 6 T. Films with lower 211 layer thickness had increased self-and-intermediate-field J_cs; e.g. ~30% average increase comparing 211 ~0.5 to nm–⩾1.0 nm, similar to results on single crystal substrates [15]. Self-field J_cs were the same for films deposited on Ni–W and Ni substrates prepared at all three labs.

The question of whether the pinning enhancements in Fig. 3(a) on RABiTS substrates were the same as on single crystal substrates was better addressed in Fig. 3(b), which compares $J_c(H)$/$J_c(0\ \mathrm{T})$ plots of multilayer and 123-only films deposited on both substrates. Fig. 3(b) indicates that the normalized $J_c(H)$ for multilayers was the same for both substrates at least for fields up to 2 T. The only effect of the RABiTS substrates was to decrease the self-field J_cs; e.g. from about 4–5 MA/cm^2 on single crystal substrates to about 1.3–1.5 MA/cm^2 on RABiTS for both multilayer (211~0.5 nm) and 123-only films. The 123-only films had slightly better (relative) pinning at intermediate fields 1–3 T on RABiTS compared to single crystal substrates. Both multilayer and 123-only films had poorer $J_c(H)$ performance at higher fields (>6 T) on RABiTS compared to single-crystal substrates.

To fully understand how the $J_c(H)$ properties correlate to the microstructure of the multilayer films on RABiTS substrate, the $J_c(H)$ intragrain properties on every type and orientation of Ni grains must be known, as well as the effect of 211 nanoparticle addition on grain boundary transport mechanisms. Such detailed information is presently not available, therefore it is not possible to predict the full-sample-length $J_c(H)$ results on RABiTS substrates shown herein. The primary conclusion that can be reached from the present studies is to understand that changing the templates did not significantly change the $J_c(H)$ properties of the multilayer films, compared to those measured on single crystal substrates. The summation of $J_c(H)$ properties across many different Ni grains and grain orientations is remarkably close to the results expected from $J_c(H)$ measured on single crystal substrates, assuming the normal decrease of J_c expected from grain misorientations on RABiTS substrates [4]. Assuming the intragrain multilayer $J_c(H)$ properties were not strongly affected by different Ni grain orientations or averaged by a distribution of negative or positive $J_c(H)$ variances, this also indirectly suggest the addition of nanoparticles does not strongly affect the grain boundary transport current limiting mechanisms which are already known [4].

4. Conclusions

In conclusion, the $J_c(H)$ properties of $(211/123) \times N$ multilayer films on RABiTS substrates showed significant increases >6-fold compared to 123-only films. Normalized $J_c(H)/J_c(0\,\mathrm{T})$ plots indicate the pinning performance was neither (further) enhanced nor decreased as a consequence of switching templates from single-crystal to RABiTS substrates. While moderate-to-severe microstructural differences were observed on the RABiTS substrates particularly with enhanced void formations, the differences apparently did not have great effect on the overall pinning performance. For example, while current flows might have been restricted across selected grains, enhancements might have occurred with other grains to offset those effects.

Acknowledgements

The authors would like to thank Marty Rupich and American Superconductor Corporation for supplying buffered Ni–W substrates, Ken Marken and Oxford Instruments for supplying textured Ni substrates, and J. Murphy, L. Brunke, and J. Tolliver at AFRL for high-field J_c measurements.

References

[1] P.N. Barnes, G.L. Rhoads, J.C. Tolliver, M.D. Sumption, K.W. Schmaeman, IEEE Trans. Magn. 41 (2005) 268–273.
[2] J.L. MacManus-Driscoll, S.R. Foltyn, Q.X. Jia, H. Wang, A. Serquis, L. Civale, B. Maiorov, M.E. Hawley, M.P. Maley, D.E. Peterson, Nature Mater. 3 (2004) 439.
[3] J.L. MacManus-Driscoll, S.R. Foltyn, Q.X. Jia, H. Wang, A. Serquis, B. Maiorov, L. Civale, Y. Lin, M.E. Hawley, M.P. Maley, D.E. Peterson, Appl. Phys. Lett. 84 (2004) 5329.
[4] D. Larbalestier, A. Gurevich, D. Matthew Feldmann, A. Polyanskii, Nature 414 (2001) 368.
[5] Y. Iijima, K. Onabe, N. Tugaki, N. Tanabe, N. Sadakara, O. Kohno, Y. Ikeno, Appl. Phys. Lett. 60 (1992) 769.
[6] X.D. Wu, S.R. Foltyn, P.N. Arendt, W.R. Blumenthal, I.H. Campbell, J.D. Cotton, J.Y. Coulter, W.L. Hults, M.P. Maley, H.F. Safar, J.L. Smith, Appl. Phys. Lett. 67 (1995) 2397.
[7] A. Goyal et al., US patent No: 5,739,086; 5,741,377; 5,846,912; 5,898,020.
[8] A. Goyal, D.P. Norton, J.D. Budai, M. Paranthaman, E.D. Specht, D.M. Kroeger, D.K. Christen, Q. He, B. Saffian, F.A. List, D.F. Lee, P.M. Martin, C.E. Klabunde, E. Hatfield, V.K. Sikka, Appl. Phys. Lett. 69 (1996) 1795.
[9] A. Goyal et al., US patent No: 5,964,966; 6,106,615; 6,451,450.
[10] A. Goyal, D.F. Lee, F.A. List, E.D. Specht, R. Feenstra, M. Paranthaman, X. Cui, S.W. Lu, P.M. Martin, D.M. Kroeger, D.K. Christen, B.W. Kang, D.P. Norton, C. Park, D.T. Verebelyi, J.R. Thompson, R.K. Williams, T. Aytug, C. Cantoni, Physica C 357–360 (2001) 903.
[11] A. Goyal, R. Feenstra, M. Paranthaman, J.R. Thompson, B.Y. Kang, C. Cantoni, D.F. Lee, F.A. List, P.M. Martin, E. Lara-Curzio, C. Stevens, D.M. Kroeger, M. Kowalewski, E.D. Specht, T. Aytug, S. Sathyamurthy, R.K. Williams, R.E. Ericson, Physica C 382 (2002) 251.
[12] S.R. Foltyn, E.J. Peterson, J.Y. Coulter, P.N. Arendt, Q.X. Jia, P.C. Dowden, M.P. Maley, X.D. Wu, D.E. Peterson, J. Mater. Res. 12 (1997) 2941.
[13] U. Balachandran, B. Ma, M. Li, B.L. Fisher, R.E. Koritala, D.J. Miller, S.E. Dorris, Physica C 392–396 (2003) 806.
[14] T. Haugan, P.N. Barnes, I. Maartense, E.J. Lee, M. Sumption, C.B. Cobb, J. Mat. Res. 18 (2003) 2618.
[15] T. Haugan, P.N. Barnes, R. Wheeler, F. Meisenkothen, M. Sumption, Nature 430 (2004) 867.
[16] T. Haugan, P.N. Barnes, L. Brunke, I. Maartense, J. Murphy, in: A. Goyal, Y. Kuo, O. Leonte, W. Wong-Ng (Eds.), Epitaxial Growth of Functional Oxides, The Electrochemical Society, Pennington NJ, 2005.
[17] T. Haugan, P.N. Barnes, L. Brunke, I. Maartense, J. Murphy, Physica C 397 (2003) 47.
[18] J. Wu et al., AFOSR Coated Conductor Review, St. Petersburg FL, January 2004, Draft paper.